# In situ ATR-FTIR and SFM Studies on the Influence of Adsorption time on Deposition and Nanostructure of Poly(ethyleneimine)/Poly(acrylic acid) Multilayers

*M. Müller,* S. Paulik*

**Summary:** The deposition and the nanostructure of polyelectrolyte multilayers (PEM) of branched poly(ethyleneimine)/poly(acrylic acid) (PEI/PAC) was studied in dependence of the adsorption time ($t_{ADS}$) of the individual steps. PEM were reproducibly deposited applying up to $z = 20$ adsorption steps at the fixed pH combination of 10/4 and polyelectrolyte concentration $c_{PEL} = 0.005$ M in a flow cell using an automated valve system. in situ ATR-FTIR spectroscopy and SFM were used for quantitative determination of deposited amount and thickness, respectively. A linear relation between PEL band integrals and thickness of thin PEM films was found. Varying $t_{ADS}$ from 0.5 to 5 min in each of the adsorption steps resulted in a steep rise of the deposited PEM amount. For $t_{ADS} > 5$ min the deposition did only marginally increase. Evidence for the release of outermost located PEI upon PAC immersion (even step) and of outermost PAC upon PEI immersion (odd step) was obtained. SFM images on consecutively deposited PEM-6 showed a slight increase in structure size and roughness for increasing $t_{ADS}$. These studies help to prepare polyelectrolyte based films with controlled thickness for the interaction with biofluids in the biomedical and food field.

**Keywords:** ATR-FTIR; deposition; poly(acrylic acid); poly(ethyleneimine); polyelectrolyte multilayers; SFM

## Introduction

Polyelectrolyte (PEL) multilayers (PEM) can be used as a simple surface modification technique for curved and planar substrates based on aqueous systems. PEM were introduced by Decher[1] in the early nineties and have become an interesting topic of colloid and surface science, which is comprehensively reviewed therein.[2–4] PEM have wide application fields in biomedicine,[5–8] diagnostics and sensorics,[9–11] and separation technology.[12–14] In principle, the PEM deposition process is based on the consecutive adsorption of polycations (PC) and polyanions (PA), typically on charged substrates beginning with the oppositely charged PEL. Although the preparation of PEM can be easily performed, fundamental issues like overcompensation and growth mechanism, location of the counterions, internal PEL order and composition, surface morphology and longterm stability of PEM are still not completely resolved. Concerning PEM growth mechanism the traditional picture is based on the linear relation between the UV absorbance of one PEM component like poly(styrene sulfonate) and the bilayer number, from which a well defined regular PEL uptake of a constant thickness increment was derived.[1] From the beginning of 2000 this picture was partly reviewed by the observation of exponential growth in certain systems, especially when charged polypeptides like poly(L-lysine) or poly (L-glutamic acid) were involved,[15,16] which was explained by diffusion of PEL ''in'' and ''out'' of the PEM. A three zone model of

Leibniz Institute of Polymer Research Dresden e.V. (IPF Dresden), Department of Surface Modification, Hohe Straße 6, 01069 Dresden, Germany
E-mail: mamuller@ipfdd.de

PEM[17] was propagated claiming a non-stoichometric zones for the surface (I) and the outermost region (III) and a 1:1 stoichometry in the core zone II between I and III. Recently, the PEM deposition process was found to consist of both uptake of the incoming immersed PEL and rupture of the previously adsorbed PEL by the respective oppositely charged PEL, as it was convincingly shown by Cohen-Stuart.[18] While they used reflectometry to show that upon immersing the new PEL solution an initial overall thickness decrease occurs, systematic studies are lacking on molecular composition changes.

In this paper we focus on the deposition and molecular composition of a PEM system consisting of commercially available branched poly(ethyleneimine) (PEI) and poly(acrylic acid) (PAC) using quantitative *in situ* attenuated total reflexion Fourier transform infrared (ATR-FTIR) spectroscopy and scanning force microscopy (SFM). While accumulated knowledge from the literature is available on the influence of parameters like chain charge,[19] ionic strength[20–22] and pH,[23,24] on PEM deposition the influence of adsorption time has not been systematically studied yet. Herein the influence of the adsorption time in every individual adsorption step is focussed at. Therefore, as main parameter the adsorption time of each of the respective deposition steps was varied, while pH and PEL concentration were kept constant.

## Experimental Part

### Materials

Commercial branched poly(ethyleneimine) (PEI, 750.000 g/mol, branching degree: 65%[25]) from Sigma-Aldrich (Steinheim, Germany) and linear poly(acrylic acid) (PAC, 50.000 g/mol) from Polysciences Inc. (Warrington, U.S.A.) were used. Polyelectrolyte (PEL) solutions were prepared by dissolving in Millipore water at concentrations of $c_{PEL} = 0.005$ M. The pH values of the unbuffered polyelectrolyte solutions were $10.0 \pm 0.1$ for PEI and $4.0 \pm 0.2$ for PAC solution, respectively. Trapezoidal silicon internal reflection elements (IRE, $50 \times 20 \times 2$ mm$^3$) were purchased from Komlas GmbH (Berlin, Germany), which were at first placed in a mixture of $H_2SO_4/H_2O_2$ (50/50 v/v%), then in water, alcohol and chloroform and finally were cleaned by UV plasma under reduced pressure (plasma cleaner/sterilizer PDC-32 G, Harrick, Ossining, NY, U.S.A.) to remove organic impurities and create reproducible surface properties.

### PEM Depositon

PEM were prepared by injecting consecutively in that sequence PEI solution at pH = 10, pure water, PAC solution at pH = 4 at a concentration of $c_{PEL} = 0.005$ M into the S compartment (see below) of the *in-situ*-ATR cell as it is shown in the Figure 1.

An automated valve system[26] (M.M., W. Jenschke, IPF Dresden e.V., Wünschmann GmbH, Dresden) triggering the IR spectroscopic measurements was used, by which flow (mL/min) and adsorption time (min) could be varied according to the following protocol: (i) Injection of PEI solution at a flow of 40 mL/min for 10 sec, then further adsorption at a flow of 1 mL/min for 5 min, (ii) injection of Millipore water (flow: 40 mL/min) for 10 sec, then further rinsing (flow: 1 mL/min) for 150 sec

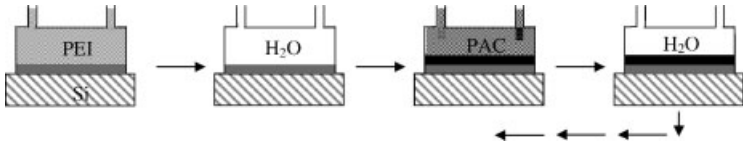


***Figure 1.***
Polyelectrolyte multilayer (PEM) deposition in the *in-situ* ATR cell (grey: polycation solution (PC), black: polyanion solution (PA), white: Millipore water ($H_2O$).

 

and IR measurement, (iii) injection of PAC solution (flow: 40 mL/min) for 10 sec, then further adsorption (flow: 1 mL/min) for 5 min, (iv) injection of Millipore water (flow: 40 mL/min) for 10 sec, then further rinsing (flow: 1 mL/min) for 150 sec and IR measurement, (v) = (i) (iterations).

### Scanning Force Microscopy

SFM measurements were performed on the Ultramiscroscope consisting of an optical microscope and SFM attachment (Nanostation II, SIS GmbH, Herzogenrath, Germany). Silicon probe tips from Nanosensors (Darmstadt, Germany) were used having radii of around 10 nm. The measurements were performed in the ''non-contact mode'' directly on the dry PEM samples on Si-IRE (internal reflection elements) used in the ATR-FTIR measurements under room conditions. The SFM images were recorded in topography, error and phase mode. As soon as artefacts (e.g. triangles as convolution of the tip with the object) appeared, the tip was immediately replaced. The scanning parameters were optimized by minimizing the signal in the error mode. Surface profiles were generated from SFM raw data by the SISCANPro software. The RMS roughness values were determined from the respective SFM images in the topography mode. Film thickness was measured based on topography images ($32 \times 32$ μm) of zones treated by careful scalpel cuts considering the height difference between undamaged film and bare silicon.

### in situ ATR-FTIR Spectroscopy

The principle of in situ attenuated total reflection Fourier transform infrared (ATR-FTIR) spectroscopy is given in the Figure 2. ATR-FTIR measurements were performed on the in situ ATR-FTIR apparatus (Optispec, Zürich, Switzerland), which was installed on a FTIR spectrometer (IFS 55, Bruker Optik GmbH, Leipzig, Germany). This attachment consists of a special mirror setup and a transparent *in situ* sorption cell (M.M., IPF Dresden e.V.) using a plasma cleaned silicon internal reflection element (Si-IRE). ATR-FTIR absorbance spectra were recorded by the single-beam-sample-reference (SBSR) technique[27] based on probing separately the upper sample (S) and lower reference (R) half of a trapezoidal Si-IRE ($50 \times 20 \times 2$ mm$^3$, N = 11 active reflections on the shorter side), which was sealed by O-rings and front and back side of the in-situ cell, by a single IR beam. Wavenumber dependent intensities recorded for S $I_S(\nu)$ were devided by those for R $I_R(\nu)$ and the absorbance was computed by $A_{SBSR} = -\log\,(I_S(\nu)/I_R(\nu))$. Typically, the in situ ATR-FTIR measurements on the consecutive deposition of PEI/PAC were triggered on-line by the automated

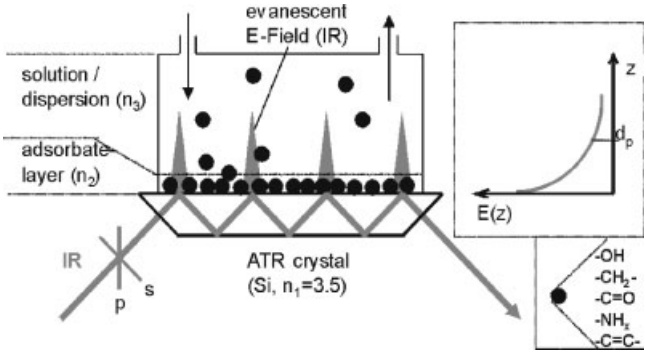


***Figure 2.***
Principle of in-situ ATR-FTIR spectroscopy featuring exponentially decaying evanescent waves at the optically dense/rare medium interface to probe surface attached organic material. (From[28] with kind permission).

 

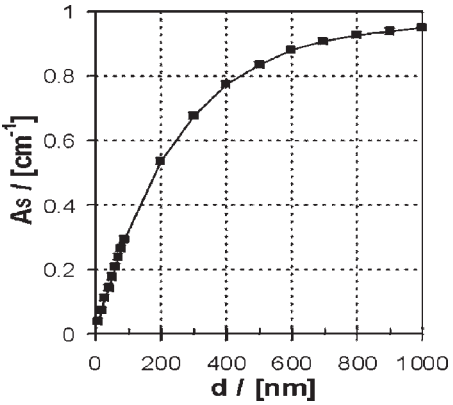


***Figure 3.***
Course of the ATR measured absorbance $A_S$ in dependence of the variable layer thickness d according to Equation (1) and (2) using arbitrary constant values for N, $\varepsilon$ and c. (From[28] with kind permission).

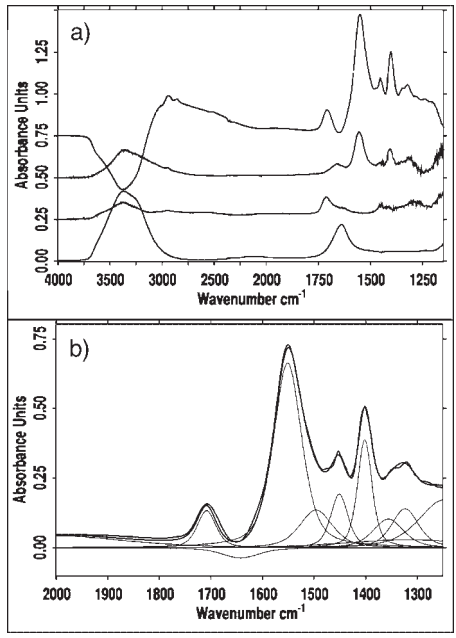


***Figure 4.***
a) ATR-FTIR spectra of liquid water (scaled by 0.5), 1 M PAC at pH = 2, 1 M PAC at pH = 10 and PEM-10 in contact to Si-IRE (bottom to top). b) Lineshape analysis results on a typical PEM spectrum (PEM-10) using nine positive and one negative Lorentzian/Gaussian (50/50%) component at 1643 $cm^{-1}$ ($\delta$(OH)) (constraint fit).

valve system. ATR-FTIR spectra (50 scans were coadded) were always recorded after rinsing the respective PEI or PAC solution out of the sample compartment by Millipore water (see protocol above). The spectral resolution was 2 $cm^{-1}$. No significant spectroscopic changes were observed comparing ATR-FTIR spectra recorded in the presence of PEI or PAC solution with those recorded after rinsing and in the presence of Millipore water.

**Processing of the ATR-FTIR Data**

In the ATR-FTIR spectra on (especially thick) PEM films in liquid water at the silicon IRE surface a negative $\nu$(OH) stretching band at around 3380 $cm^{-1}$ as well as a negative $\delta$(OH) band at 1643 $cm^{-1}$ appeared shown in the Figure 4a, which is due to the lower concentration or removal of liquid water at the modified IRE surface, as it will be pointed out later. (Other spectra in Figure 4a are explained below).

Since especially the negative $\delta$(OH) band overlaps the diagnostic $\nu$(C=O) and $\nu(COO^-)$ bands of poly(acrylic acid) (see below), this band has to be taken into account for an exact data analysis. This problem was addressed by lineshape analysis (LSA) in the range from 2000–1250 $cm^{-1}$, representing the lineshape by the superposition of ten Lorentzian/Gaussian (50%/50%) bands. At first LSA was performed under free relaxation of the parameters (wavenumber) position, halfwidth and intensity for nine components and all PEM-z spectra (z = 2 to 20). As tenth component a negative $\delta$(OH) band at 1643 $cm^{-1}$ with a halfwidth of 85 $cm^{-1}$, whose parameters were found by fitting a bulk water spectrum (Figure 4a, bottom spectrum), was kept fixed and only the (negative) intensity was relaxed. This procedure evidenced nine further positive components at 1250, 1323, 1354, 1402, 1451, 1490, 1552, 1707 and 2000 $cm^{-1}$, which could be also identified by visual inspection. Note that the 1250 and 2000 $cm^{-1}$ components were used as ''dummy'' components to avoid boundary effects on the intensities

 

of the critical 1707, 1643 and 1552 $cm^{-1}$ components. Then the respective positions and halfwidths of all peaks were averaged and in a second run all these spectra were fitted fixing the averaged values of position and halfwidth and relaxing solely the intensities (constraint fit). A representative constraint fit result is shown for PEM-10 in the Figure 4b, featuring the original and simulated lineshape and the ten overlapping components.

### Quantitative Analysis of the ATR-FTIR Data

Exact quantitative ATR-FTIR analysis is based on a modified Lambert-Beer law given in Equation (1):

$$A_S = N\,\varepsilon\,c\,d_{E,S} \quad (1)$$

including the integrated absorbance of a given IR band measured in s-polarization $A_S$ [$cm^{-1}$], number of active reflections N, absorption coefficient $\varepsilon$ [cm/Mol], concentration c [$Mol/cm^3$], and the effective thickness $d_{E,\,S}$ [$cm^{-1}$] due to Harrick,[29] which is given by:

$$d_{E,S} = n_2\,d_p\,E_Y^2/(2\cos\theta\,n_1) * [1 - \exp(-2d/d_p)] \quad (2)$$

$d_{E,\,S}$ is a function of the refractive indices of the involved media $n_1$ (Si, 3.5), $n_2$ (PEM, 1.5) and $n_3$ (water, 1.33), incident angle of IR beam $\theta$ (45°), thickness d and the >penetration depth $d_P$ (≈260 nm at 3000 $cm^{-1}$, 460 nm at 1700 $cm^{-1}$ and 510 nm at 1550 $cm^{-1}$) and the relative electrical field component in y-direction $E_Y = 2\cos\theta/(1-(n_3/n_1)^2)^{1/2}$. The surface concentration $\Gamma$ [$Mol/cm^2$] can be obtained from by inserting c from (1) into following Equation (3):

$$\Gamma = c\,d \quad (3)$$

A typical course of the measured absorbance $A_S$ of an organic layer system in dependence of its thickness d is given in the Figure 3. Two points are characteristic: At first for thin films between $d = 0$ up to 300 nm a quasi linear dependence of $A_S$ on d can be approximated. Secondly, for thick films $A_S$ runs into a saturation, meaning that the ATR-FTIR method gets increasingly insensitive to additional layer deposition or the nature of outer film regions, when d exceeds penetration depth $dp \approx 500$ nm. For the semiquantitative determination of $\Gamma$ the integrated areas of typical polyelectrolyte (PEI, PAC) IR bands A, which were measured by unpolarized IR beam, were considered. For the determination of PEI surface concentration the integral of the $\nu$(CH) band at 2855 $cm^{-1}$ (limits: 2890–2820 $cm^{-1}$) was used denoted as $A_{CH}$ (=$A_{PEI}$). For the PAC surface concentration the integral of the $\nu$(C=O) component ($A_{C=O}$) at 1707 $cm^{-1}$ and of the $\nu(COO^-)$ component ($A_{COO^-}$) at 1552 $cm^{-1}$ were used according to the relation $A_{PAC} = F \cdot A_{C=O} + A_{COO^-}$. In that work $F = 2.24$ was used, which is due to the ratio of the absorption coefficients of $\nu(COO^-)$ and $\nu$(C=O) band. This ratio can be obtained from the spectra of 1 M PAC at pH = 2 (only $\nu$(C=O)) and at pH = 10 (only $\nu(COO^-)$), respectively, which are given in the Figure 4a (above). These integrals $A_{PEI}$ and $A_{PAC}$ are approximately proportional to the surface concentration (denoted further as deposited amount) of PEI and PAC, respectively, if the overall thickness of the PEM film $d < 300$ nm (see Figure 3). Otherwise for $d > 300$ nm the PEL deposited amount is increasingly underestimated for increasing PEM thicknesses. For relative comparisons normalized values of $A^N_{PEI}$ and $A^N_{PAC}$ were used, whereby the actual $A_{PEI}$ or $A_{PAC}$ value was devided by the corresponding value obtained for an adsorption step $z \gg 10$, where the respective band integral was in saturation (no further signal increase in dependence of z).

## Results and Discussion

In the following results on the characterization of consecutively adsorbed PEM consisting of branched PEI and PAC at silicon IRE at a fixed pH setting and constant $c_{PEL}$, which were obtained by

 

ATR-FTIR spectroscopy and SFM, will be presented. The main parameter studied was the adsorption time $t_{ADS}$. Branched PEI was chosen, since it was expected to result in higher deposited amounts compared to linear PEI. ATR-FTIR spectroscopy was used to determine deposited amount and chemical composition in dependence of $t_{ADS}$, while SFM performed on the samples previously measured by ATR-FTIR gave informations on the formed nanostructures in dependence of $t_{ADS}$.

The paper is structured as follows: At first typical *in-situ*-ATR-FTIR spectra on consecutive PEI/PAC deposition in dependence of the adsorption step z are presented and assignments of typical IR bands related selectively to PEI and PAC, respectively, are given. Secondly, deposition profiles, i.e. courses of typical band integrals in dependence of $t_{ADS}$ and interpretations of their non trivial courses are given. Thirdly, SFM images on equivalent samples previously characterized by ATR-FTIR are presented illustrating the influence of $t_{ADS}$ on PEM nanostructure. Finally, the results are discussed and conclusively summarized.

## ATR-FTIR Spectra

Typical ATR-FTIR spectra on the consecutive deposition of PEI and PAC on Si-IRE are given in the upper part of Figure 5 for a single PEI layer ($z = 1$, PEM-1, bottom) up to twelve consecutively adsorbed PEI and PAC layers ($z = 12$, PEM-12).

As fixed parameters settings $c_{PEL} = 0.005$ M and pH $\approx 10$ (PEI) and $\approx 4$ (PAC) were chosen, since under these conditions the deposited amount was found to be highest [30]. In these original uncorrected PEM spectra the increasing overall intensity and the changes of both the $\nu$(C=O) band (carbonyl stretch) at around 1707 $cm^{-1}$ and the $\nu(COO^-)$ band (asymmetric carboxylate stretch) at 1552 $cm^{-1}$, respectively, in dependence of z are most significant, which both can be exclusively attributed to the PAC component. Moreover, a weak $\nu$(CH) band between 2890–2820 $cm^{-1}$ is important, which can be exclusively assigned to the CH and $CH_2$ moieties of PEI (Figure 5, right part). This was recently confirmed by ATR-FTIR spectra on bulk 1 M PEI compared to 1 M PAC solution therein.[30] Furthermore, an increasing negative $\nu$(OH) band at around 3380 $cm^{-1}$ shows up, which reflects the more distant location of water in contact to the PEM film (S compartment) compared to the bare Si-IRE (R compartment) with respect to the Si surface. Hence the $\nu$(OH) band senses film formation as the removal of water from the surface in

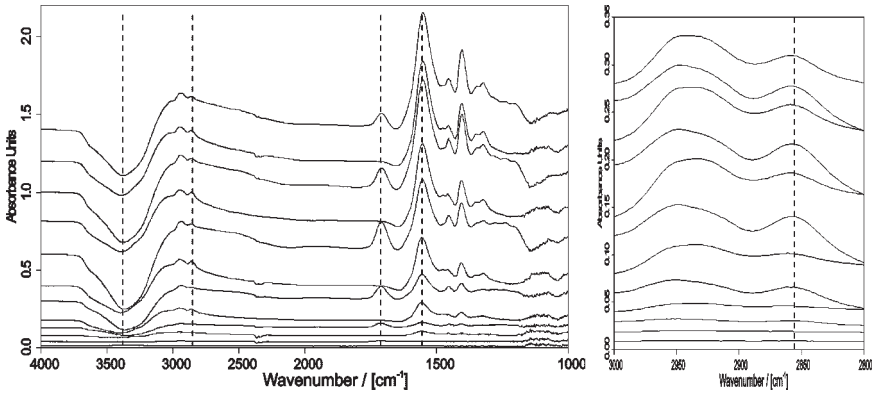


***Figure 5.***
Left: Original *in-situ*-ATR-FTIR spectra (uncorrected data, see Experimental) on the consecutive deposition of PEM from solutions of PEI at pH $\approx 10$ and PAC at pH $\approx 4$ for $c_{PEL} = 0.005$ M and $t_{ADS} = 5$ min onto Si-IRE. PEM-z are shown from $z = 1$ to 12 from bottom to top. Right: respective extended $\nu$(CH) spectral regions (PEI). Typical IR bands used for further analysis are indicated by vertical broken lines (see text).

 

*Table 1.*
Assignment of IR bands and lineshape components appearing in ATR-FTIR spectra of PEM-PEI/PAC.

| Wavenumber/[cm$^{-1}$] | Assignment | Component |
|---|---|---|
| 3380 | $\nu$(OH) | $H_2O$ |
| 2955 | $\nu$(CH) | PEI |
| 1707 | $\nu$(C=O) | PAC |
| 1643 | $\delta$(OH) | $H_2O$ |
| 1552 | $\nu_a$(COO$^-$) | PAC |

dependence of the adsorption step z. A summary of selected IR bands or the fitted band components (see above) used in this study and their assignment is given in the Table 1.

## Deposition Profiles

The integrated areas of the selected IR bands were used to quantify PEM-PEI/PAC deposition. Most relevantly, the $\nu$(CH) band at 2855 cm$^{-1}$ ($A_{CH}$) can be used as a direct diagnostic measure for the deposited amount of PEI, while for the deposited amount of PAC the fitted band components $\nu$(C=O) ($A_{C=O}$) and $\nu_a$(COO$^-$) ($A_{COO^-}$) have to be considered. In the Figure 6 typical courses of the integrals of $\nu$(COO$^-$), $\nu$(C=O), $\nu$(CH) and $\nu$(OH) band versus the adsorption step z are given, which are discussed in the following:

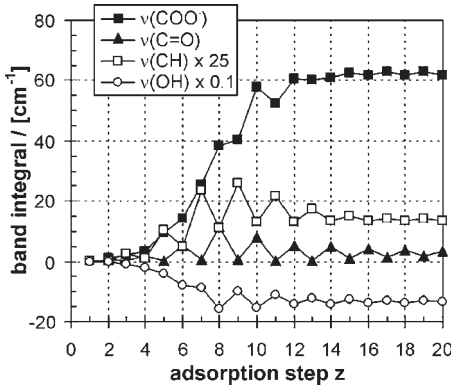


*Figure 6.*
Courses of the integrals of the $\nu$(CH) band at 2855 cm$^{-1}$ (white cubes) assigned to PEI, the fitted $\nu$(C=O) and $\nu$(COO$^-$) band components at 1707 and 1552 cm$^{-1}$ (black triangle, cube) assigned to PAC and the $\nu$(OH) band (white circle) of water versus z measured during consecutive PEM-z deposition from PEI/PAC solutions for pH $\approx$ 10/4, $c_{PEL} = 0.005$ M and $t_{ADS} = 5$ min onto Si-IRE. The given band integrals are based on ATR-FTIR sprectra, which were corrected for the negative $\delta$(OH) band at 1640 cm$^{-1}$ (see Experimental).

### *$\nu$(COO$^-$) Band Component*

The course of the $\nu$(COO$^-$) band component ($A_{COO^-}$) due to PAC shows after a certain quasi linear lag phase until around z = 4 a steep rise and an asymptotic behaviour for the adsorption steps z = 5–20. This is primarily due to the ATR-FTIR mode, which senses lateral PEM deposition as a linear function of A versus z, while vertical PEM deposition is sensed as an exponentially damped function given in Equation (1) and drawn in the Figure 3 (Experimental section). Hence, we conclude a short initial phase of mainly lateral growth up to z = 4, followed by a mainly vertical PEM deposition from z = 5–20.

### *$\nu$(C=O) Band Component*

For the $\nu$(C=O) band components ($A_{C=O}$) due to PAC a non trivial course was found. In the modulated course of $A_{C=O}$, the values for even steps were always higher compared to the odd step before and after. This is generally due to a periodic uptake and loss of carboxylic acid (COOH) groups. Thereby the COOH group decrease in the odd steps can be caused either by deprotonation or also by the loss of PAC molecules. Since COOH and COO$^-$ groups are complementary, the deprotonation of COOH should result in a gain of COO$^-$ groups. However, since e.g. the decrease of $A_{C=O}$ from z = 8 to z = 9 is not paralleled by a corresponding rise of $A_{COO^-}$, we conclude, that predominantly protonated PAC is released in every PEI step. Hence from both modulated courses PEM loss tendencies were found, when either PEI or PAC is immersed on the actual PEM-z to create PEM-(z + 1). Furthermore $A_{C=O}$ shows a transient behaviour with a maximum at z = 8, which is due to the ATR-FTIR sensing characteristics: i.e. at

 

$z = 8$ there is a maximum of COOH groups sensed, while for subsequent steps $z = 10$, 12–20, even assuming a similar number of COOH groups in the outermost region, a smaller $A_{C=O}$ value was measured. From that we conclude on the one hand a considerable accumulation of PAC at the outermost PEM surface region. On the other hand for $z = 8$ the roughness of the PEM film could enable the PAC solution to contact PEM regions of small thickness or even the bare silicon surface, so that the evanescent field for PEM-8 senses PAC stronger compared to PEM-20, where accumulated PAC is no longer near the silicon surface or in the region of stronger evanescent field (see also $\nu$(CH) band below).

*$\nu$(CH) Band*

For the band integrals of $\nu$(CH) due to PEI (further denoted as $A_{PEI}$) also a non trivial course was found. First of all strong modulation features can be identified, so that for PEI in every odd step $A_{CH}$ was higher compared to the even step before and after. This modulated course of $A_{CH}$ is due to a periodic uptake of PEI material for the odd PEI steps $z = 1$–19 and a respective loss of PEI material for the even PAC steps $z = 2$–20. From this we conclude that the initially bound PEI is partly released by the oppositely charged PAC into solution. Secondly very interestingly, in the Figure 6 the maximum $A_{CH}$ value for $z = 9$ ($\approx$26 $cm^{-1}$) is higher compared to the saturation value ($\approx$14 $cm^{-1}$) at $z = 20$ by a factor of nearly 2. Hence, considering a thickness increment from 0 to 500 nm, which is about in the range of the penetration depth (see Experimental), a higher PEI amount can be concluded for thinner PEM-9 at 0.005 M, where mainly the outermost bound PEI amount is sensed, compared to thicker PEM-19, where mainly the internally bound PEI amount is sensed. Analogously to the findings for $A_{PAC}$, this means that in the outermost regions of e.g. PEM-19 a similar large PEI uptake may take place, but within the given thickness increment this is no longer detected by ATR-FTIR. At that point it has to be noted, that the difference of the refractive indices for water ($n_3 = 1.33$) dominating for PEM-9 and for the PEM film ($n_2 = 1.5$) dominating for PEM-20 could not cause this absorbance difference. According to Harrick[29] an increase in $n_2$ should rather result in a higher $A_{CH}$ value by some factor of 1.09. These results can be interpreted based on two models, which may interfere somehow. On the one hand the outermost region of this PEM type may always consist of a huge amount of accumulated excess PEI, which is exceeding the internally bound amount by far. On the other hand the PEM may always be in a highly eroded state, so that until a certain z the PEI solution may still contact regions of bare silicon substrate sensed maximum by ATR-FTIR. The first interpretation would be in line with an accepted three zone model,[17,31] where the outermost zone is claimed to be highly nonstoichiometric, while in the internal bulk zone 1:1 stoichiometry prevails. In the respective subsequent steps this excess PEL amount is desorbed to a high degree, which can be seen by the huge modulation amplitude for PEI/PAC. However, the true picture accounts additionally for highly eroded PEM (second interpretation), where the three zone model is only locally valid. This point will be addressed in the morphology part below.

*$\nu$(OH) Band*

Finally, in the Figure 6 also the modulated course of the negative $\nu$(OH) band is given, which reflects the location of water with respect to the bare silicon surface or the sensing evanescent field. Significantly, in the odd PEI steps the integral of the $\nu$(OH) band ($A_{H2O}$) is always higher compared to the even PAC steps before and after. This tendency can be due to two contributions: Either outermost PEI layers are more hydratable compared to outermost PAC layers, or in the PEI steps the thickness or deposited amount of the whole PEM is always smaller compared to the PAC step before and after. A detailed interpretation will be published therein.[30]

 

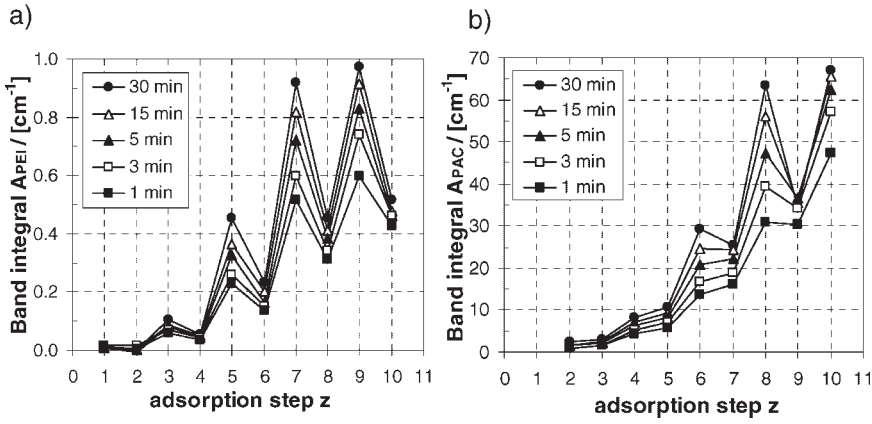


***Figure 7.***
a) $A_{PEI}$ of PEM-z plotted versus adsorption step z = 1 to 10 for $t_{ADS}$ = 0.5, 1, 3, 5, 15, 30 min (indicated). b) $A_{PAC}$ of PEM-z plotted versus adsorption step z = 1 to 10 for $t_{ADS}$ = 0.5, 1, 3, 5, 15, 30 min (indicated).

**Influence of Adsorption Time $t_{ADS}$**

Furthermore, PEM deposition was studied varying the adsorption time $t_{ADS}$. In the Figure 7a the courses of $A_{PEI}$ and in the Figure 7b those of $A_{PAC}$ are shown in dependence of the adsorption step for various $t_{ADS}$ values related to the individual adsorption steps. $A_{PAC}$ was calculated according to $A_{PAC} = F \cdot A_{C=O} + A_{COO^-}$ (see Experimental) to address the total PAC amount. The $A_{PEI}$ and $A_{PAC}$ courses reflect the actual uptake and release of PEI and PAC, respectively, at the support surface. In both sets of deposition profiles a significant increase of both the overall deposited amount and of the uptake/release amplitudes in dependence of $t_{ADS}$ is seen. These uptake/release tendencies for PEI and PAC are in line with results from studies of Cohen-Stuart and coworkers [18], who reported similar tendencies for a different system. As it was also claimed therein, obviously, the PEM deposition process is kinetically controlled.

As a summary, Figure 8a shows the direct dependence of the band integrals $A_{PEI}$ and $A_{PAC}$ measured for PEM-6 on $t_{ADS}$. The courses take initially a steep ascent until $t_{ADS} \approx 5$ min, followed by a less steep one. Practically, this means

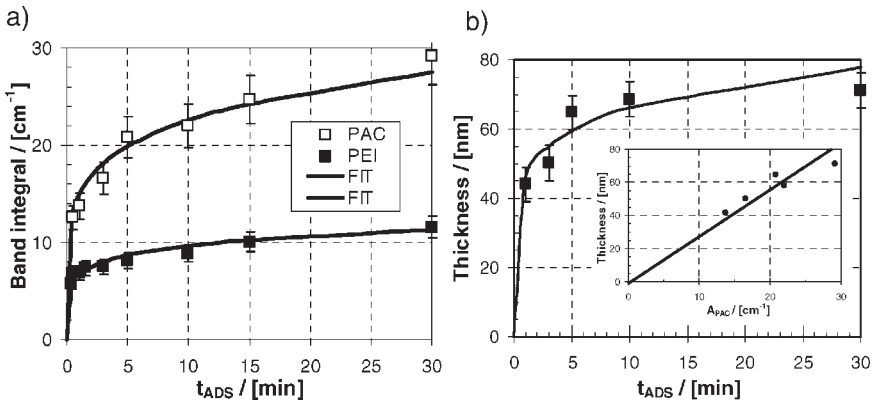


***Figure 8.***
a) $A_{PEI}$ (×50) and $A_{PAC}$ of PEM-6 plotted versus $t_{ADS}$. The full lines are fitting curves using Equation (4). b) Thickness values of PEM-6 (SFM line cut method) plotted versus $t_{ADS}$ (full lines: Fit by Equation (4)). Inlet: thickness (SFM plotted versus $A_{PAC}$ (ATR-FTIR).

 

that $t_{ADS} \approx 5$ min is sufficient for that PEM type under the chosen pH and $c_{PEL}$ conditions to obtain an effective PEM deposition. Empirically, in the given range of $t_{ADS} = 0.33$–30 min the deposited amount scales with $t_{ADS}$ by an empirical Smoluchowski like function (4) suggesting an aggregation related deposition process:

$$A = A_0\, t_{ADS}b \quad (4)$$

Fitting the experimental data of both band integrals $A_{PEI}$ and $A_{PAC}$ empirically by Equation (4) results in approximately similar b values for PEI ($b = 0.15 \pm 0.02$) and PAC ($b = 0.18 \pm 0.01$). The fitted curves are shown as black lines in Figure 8a. From that generally an aggregation type of deposition process might be speculated on and similar incorporation rates of PEI and PAC into the PEM might be concluded.

The results of Figure 8a obtained by ATR-FTIR were checked with the SFM line cut method as another sensitive analytical method delivering thickness values of the PEM films. For that the same

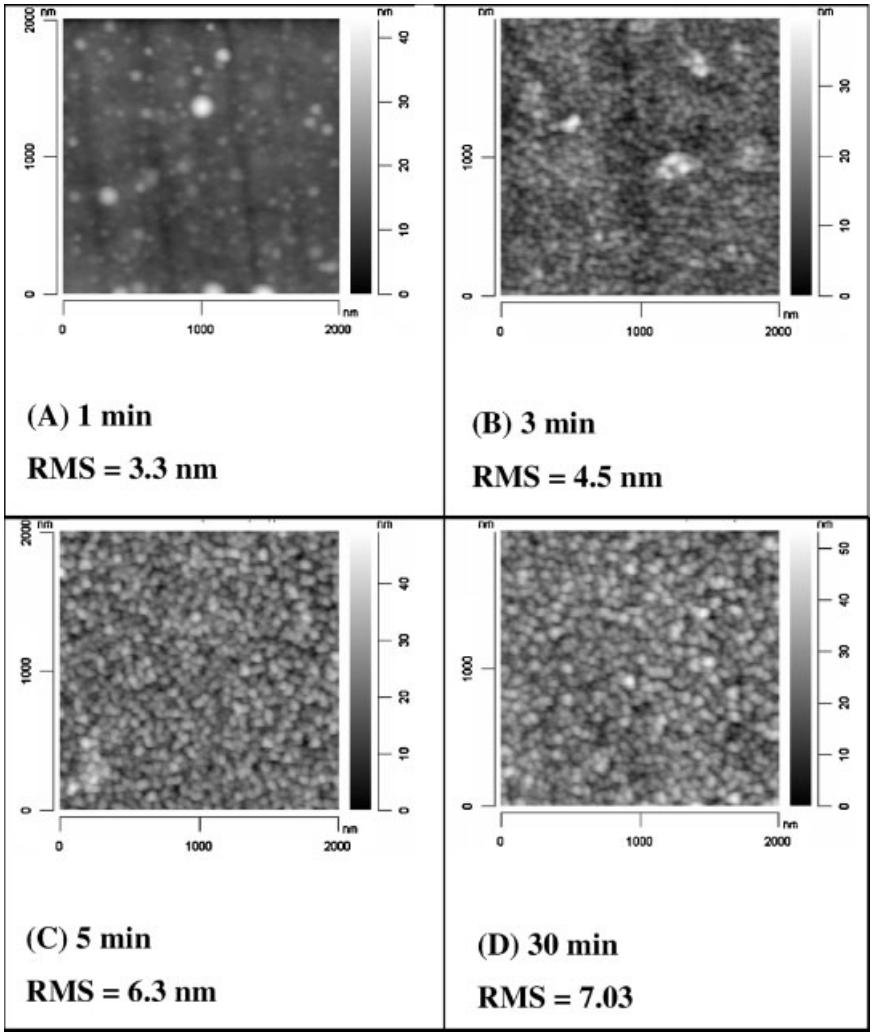


***Figure 9.***
Typical SFM images (topography) on PEM-6 samples deposited under constant pH setting of 10/4 (PEI/PAC) and $c_{PEL} = 0.005$ M for various adsorption times $t_{ADS}$.

 

PEM-6 samples as they were used in the ATR-FTIR analysis were considered. The results are shown in the Figure 8b. Significantly, a similar trend of PEM deposition in dependence of $t_{ADS}$ was found: after an additional steep rise of the thickness until $t_{ADS} = 5$ min the further thickness increase with $t_{ADS}$ is only low. Hence, practically the PEM deposition process for PEI/PAC at $c_{PEL} = 0.005$ M does not alter that much applying $t_{ADS} >$ 5 min. Hence, this value seems to be sufficient for an effective and quick process. Fitting the thickness data with Equation (4) replacing A and $A_0$ by d and $d_0$ led to $b = 0.15 \pm 0.03$, which confirms the ATR-FTIR data (the fitted curve is shown as full line). From this result it could be additionally concluded, that if thicknesses within the range 0–300 nm are studied, the band integrals obtained by ATR-FTIR analysis are approximately linear with the ''true'' thickness values obtained by SFM line cut method. This observation is supported by the inlet in the Figure 8b, where the thickness found by SFM line cut method is plotted versus the $A_{PAC}$ values of the ATR analysis. From this plot an approximate linear relationship between the observables of both methods was confirmed, which seems to be the more exact the lower the thicknesses were.

### PEM Nanostructure

The equivalent PEM samples investigated by ATR-FTIR spectroscopy were studied by scanning force microscopy (SFM) aiming at the surface morphology and roughness in depen-dence of $t_{ADS}$. For that purpose only PEM-6 samples deposited under constant pH (10/4) and $c_{PEL}$ (0.005 M) were considered. Four PEM-6 samples were chosen deposited during $t_{ADS} = 1$, 3, 5 and 30 min, and in the Figure 9 A, B, C typical SFM images of these samples are shown.

There the structures and especially their sizes were slightly changing in dependence of $t_{ADS}$. For $t_{ADS} = 1$ min (A) individually appearing dots on a relative smooth base layer were found, which changed to more continuous layers of crowded dots for $t_{ADS} = 3$ min (B). For $t_{ADS} = 5$ and 30 min (A, D) the dots were more densely packed with a tendency to merging. Generally an enlargement of the surface structure in dependence of $t_{ADS}$ could be derived. Included in the Figure 9 are roughness (RMS) values, which increase with increasing $t_{ADS}$ and correlate qualitatively with the found deposited amounts given in Figure 8b. Presumably, the more PEM grow in the vertical direction with increasing adsorption time, the more roughness is created.

## Conclusion

Quantitative ATR-FTIR spectroscopy and SFM were applied on deposition of PEM of PEI and PAC in dependence of adsorption time ($t_{ADS}$) at fixed pH and PEL concentration $c_{PEL}$ providing for selective informations on PEI ($\nu$(CH)) and PAC ($\nu(COO^-)$, $\nu$(C=O)) uptake and release, respectively, as well as on surface morphology.

Plotting band integrals of these bands versus $t_{ADS}$ showed, that the deposited amount of PEI and PAC increased steeply between $t_{ADS} = 0$ to 5 min followed by a small further increase for $t_{ADS} > 5$ min. This was confirmed by SFM profile measurements on line cuts through the PEM films providing for the PEM thickness ($d_{SFM}$). Within a thickness range from 0–100 nm the band integrals related to PEI and PAC (ATR-FTIR) were shown to be approximately linear with $d_{SFM}$ (this would be not the case for thicknesses exceeding the ATR penetration depth (see Experimental)). An empirical Smoluchowski like analytical function represented the data quite sufficiently, suggesting an aggregation type of deposition process.

From oscillations features in the deposition profiles, the release of PEI upon PAC immersion (even steps) and of PAC upon PEI immersion (odd steps) could be claimed for all applied $t_{ADS}$. From that a competition between PEL surface uptake and PEL solution complexation formation

 

can be concluded in line with studies of Cohen-Stuart and coworkers.[18]

SFM data on PEM-6 samples deposited at constant $pH = 10/4$ and $c_{PEL} = 0.005$ M in dependence of $t_{ADS}$ showed isolated structures for $t_{ADS} = 1$ min, moderately fused ones for $t_{ADS} = 3$ min and further fused ones for $t_{ADS} \geq 5$ min. Additionally, a subsequent roughness increase from around 3 to 7 nm was found.

These studies help to prepare polyelectrolyte based films with controlled thickness for the interaction with biofluids in the biomedical and food field.

*Acknowledgements:* This work has been financially supported by Deutsche Forschungsgemeinschaft (DFG) within Sonderforschungsbereich (SFB) 287 (B5).

[1] G. Decher, J. D. Hong, J. Schmitt, *Thin Solid Films* **1992**, *210*, 831.
[2] P. Bertrand, A. Jonas, A. Laschewsky, R. Legras, *Macromol. Rapid Commun.* **2000**, *21*, 319–348.
[3] M. Schönhoff, *J. Phys.: Condensed Matter* **2003**, *15*, 1781.
[4] G. Decher, J. B. Schlenoff, Eds., *Multilayer Thin Films-Sequential Assembly of Nanocomposite Materials*, Wiley-VCH, Weinheim **2003**.
[5] H. Kim, M. W. Urban, *Langmuir* **1998**, *14*, 7235.
[6] M. Müller, T. Rieser, K. Lunkwitz, S. Berwald, J. Meier-Haack, D. Jehnichen, *Macromol. Rapid Commun.* **1998**, *19*(7), 333.
[7] D. L. Elbert, C. B. Herbert, J. A. Hubbell, *Langmuir* **1999**, *15*, 5355.
[8] E. Brynda, M. Houska, M. Jirouskova, J. E. Dyr, *J. Biomed. Mater. Res.* **2000**, *51*, 249.
[9] A. Wu, D. Yoo, J. K. Lee, M. F. Rubner, *J. Am. Chem. Soc.* **1999**, *121*, 4883.
[10] E. Brynda, M. Houska, A. Brandenburg, A. Wikerstal, J. Skvor, *Biosensors and Bioelectronics* **1999**, *14*, 363.
[11] F. Caruso, F. N. Furlong, K. Ariga, I. Ichinose, T. Kunitake, *Langmuir* **1998**, *14*, 4559.
[12] P. Stroeve, V. Vasquez, M. A. N. Coelho, J. F. Rabolt, *Thin Solid Films* **1996**, 284-285, 708.
[13] F. van Ackern, L. Krasemann, B. Tieke, *Thin Solid Films* **1998**, *327–329*, 762.
[14] W. Lenk, J. Meier-Haack, *Desalination* **2002**, *148*, 11–16.
[15] E. Hübsch, V. Ball, B. Senger, G. Decher, J. C. Voegel, P. Schaaf, *Langmuir* **2004**, *20*, 1980.
[16] P. Lavalle, V. Vivet, N. Jessel, G. Decher, J. C. Voegel, P. J. Mesini, P. Schaaf, *Macromolecules* **2004**, *37*, 1159.
[17] G. Ladam, P. Schaad, J. C. Voegel, P. Schaaf, G. Decher, F. Cuisinier, *Langmuir* **2000**, *16*, 1249.
[18] N. G. Hoogeveen, M. A. Cohen-Stuart, G. J. Fleer, M. R. Böhmer, *Langmuir* **1996**, *12*, 3675.
[19] R. Steitz, W. Jaeger, R. v. Klitzing, *Langmuir* **2001**, *17*(15), 4471–4474.
[20] G. Decher, J. Schmitt, *Progr. Colloid. Polym. Sci.* **1992**, *89*, 160.
[21] X. Arys, A. M. Jonas, B. Laguitton, R. Legras, E. Wischerhoff, *Prog. Org. Coat.* **1998**, *34*, 108.
[22] M. Lösche, J. Schmitt, G. Decher, W. G. Bouwman, K. Kjaer, *Macromolecules* **1998**, *31*, 8893.
[23] D. Yoo, S. S. Shiratori, M. F. Rubner, *Macromolecules* **1998**, *31*, 4309.
[24] S. S. Shiratori, M. F. Rubner, *Macromolecules* **2000**, *33*, 4213.
[25] D. Appelhans, IPF Dresden, private communication.
[26] Patent in preparation.
[27] U. P. Fringeli, in: *Encyclopedia of Spectroscopy and Spectrometry*, J. C. Lindon, G. E. Tranter, J. L. Holmes, Eds., Academic Press, New York 2000, pp. 58–75.
[28] M. Müller, B. Keßler, W. Ouyang, *Z. Phys. Chem.* **2007**, *221*, 127–138.
[29] N. J. Harrrick, *Internal Reflection spectroscopy*, Harrick Sci. Corp., Ossining, New York 1979.
[30] M. Müller, B. Keßler, *Langmuir* 2007, (submitted).
[31] M. Castelnovo, J. F. Joanny, *Langmuir* 2000, *16*(19), 7524.

 